Proceedings of the 7th International Symposium on Cavitation
CAV2009 – Paper No. 40
August 17-22, 2009, Ann Arbor, Michigan, USA

Analytical Investigations of Thermodynamic Effect on Cavitation Characteristics of Sheet and Tip Leakage Vortex Cavitation

Satoshi Watanabe
Department of Mechanical Engineering
Kyushu University
Fukuoka, Japan

Akinori FURUKAWA
Department of Mechanical Engineering
Kyushu University
Fukuoka, Japan

Yoshiki Yoshida
Japan Aerospace Exploration Agency
Kakuda, Miyagi, Japan

Yoshinobu Tsujimoto
Graduate School of Engineering Science
Osaka University
Toyonaka, Japan

ABSTRACT

Vapor production in cavitation extracts the latent heat of evaporation from the surrounding liquid, which decreases the local temperature, and hence the local vapor pressure in the vicinity of cavity. This is called thermodynamic/thermal effect of cavitation. In the present study, the thermodynamic effect on cavitation characteristics such as cavitation compliance and mass flow gain factor, which are known to be important parameters for cavitation instabilities appearing in turbopumps, were studied. Main cavitations in turbopumps, blade and tip leakage vortex cavitations, were separately analyzed by simple analytical methods developed based on the potential flow theory, taking account of the latent heat extraction and heat transfer between the cavity and the surrounding fluid. The cavitation characteristics were estimated for the partial cavity and the tip leakage vortex cavity, and the thermodynamic effects on those characteristics were discussed.

Key words: Partial cavitation, Tip leakage vortex cavitation, Thermodynamic effect, Cavitation compliance, Mass flow gain factor

INTRODUCTION

Vapor production in cavitation extracts the latent heat of evaporation from the surrounding liquid, which decreases the local temperature, and hence the local vapor pressure in the vicinity of the cavity. Then, the development of the cavity is suppressed. This is called thermodynamic/thermal effect of cavitation. It is known that the suction performance of rocket pump inducer is much better operated with real cryogenic fluids than with cold water because of the thermodynamic effect of cavitation.

Cavitating inducer often suffers from cavitation instabilities such as rotating cavitation and cavitation surge. It has been found by Tsujimoto et al. [1] that the cavitation characteristics, cavitation compliance and mass flow gain factor, are responsible for the occurrence of the cavitation instabilities. Those cavitation characteristics have been studied theoretically by several researches [2]-[4]. Especially, Otsuka et al. [4] have succeeded in estimating the cavitation compliance and the mass flow gain factor of sheet cavity around a flat plate cascade using a conformal mapping method with a closed cavity model and clarified the frequency dependence of those cavitation characteristics. However, many of the foregoing studies treated only the sheet cavity while the other forms of cavitation such as vortex cavitation, bubble cavitation, and so on might contribute to the dynamic characteristics of real cavitating inducer, and none of them has focused on the thermodynamic effect on the cavitation characteristics. In order to achieve more reliable inducer in real cryogenic fluids, it is important to understand the cavitation characteristics under the presence of the thermodynamic effect of cavitation.

In the present study, we focus on the cavitation characteristics of major cavitations in inducer, the sheet cavitation and the tip leakage vortex cavitation. Based on the potential flow theory with the consideration of thermodynamic effect of cavitation, we have developed simple analytical methods of cavitating flow separately for unsteady sheet cavitation [5] and tip leakage vortex cavitation [6]. In this paper, the cavitation characteristics, the cavitation compliance and the mass flow gain factor, are estimated for the partial cavitation in a 2-D flat plate cascade and the tip leakage vortex cavitation of an isolated flat plate hydrofoil. Then, the thermodynamic effects on dynamic characteristics of those cavitations are discussed.

NOMENCLATURE

A_u: coefficient matrix in Eq. (12)
a: thermal diffusivity

B: blade span
C: chordlength
C_B: cavitation compliance, defined in Eq. (19)
C_p: pressure coefficient, $=2(p-p_\infty)/\rho_l U^2$
c_{pl}: heat capacity of liquid phase
f: kernel function, defined in Eq. (1)
h: blade spacing
i: imaginary unit
j: imaginary unit in time
K: cavitation compliance, defined in Eq. (13)
K_P: $=\varepsilon a/U$
k: normalized frequency, $=\omega h/U$
L: latent heat of evaporation
l: cavity length
M: mass flow gain factor, defined in Eq. (13)
M_B: mass flow gain factor, defined in Eq. (19)
$\tilde{N}$: amplitude of flow rate fluctuation
p: pressure
$\tilde{p}_0$: inlet pressure fluctuation, defined in Eq. (10)
P_V, p_v: vapor pressure
Q: unknown vector
q: source representing blade cavity
q_T: heat flux on cavity surface
q_B: source representing vortex cavity
q_J: source distribution representing tip leakage flow
R: radius of cylindrical vortex cavity
R_0: initial radius of cylindrical vortex cavity
S: coordinate along the blade
T: temperature
t: time
U: main flow velocity
U_J: leakage flow velocity
V: local evaporation velocity
V_c: cavity volume
u, v: flow velocity components in x and y directions
u_c: velocity disturbance on cavity surface
u_s, v_s: steady velocity disturbances in x and y directions
w: complex conjugate velocity
α: angle of attack
β: stagger angle
γ_1, γ_2: bound vortices representing blade
γ_J: vortex representing the shear layer of leakage flow
ΔT: temperature depression
ε: turbulent diffusion factor
η: cavity thickness
λ: thermal conductivity
ρ_L, ρ_V: densities of liquid and vapor phases
Σ^*: thermodynamic parameters, defined by Eq. (14)
σ: cavitation number
τ: tip clearance
ω: angular frequency of fluctuations
ξ: distance along the from the leading edge

Superscripts

~: amplitude of unsteady component
*: non-dimensional value using U and C

Subscripts

C, c: cavity surface
s: steady component
∞: upstream infinity

OUTLINE OF ANALYSES

In the present study, we analyze the cavitating flow in a flat plate cascade and around a tip leakage vortex, based on the potential flow theory. The thermodynamic effect of cavitation is considered in both analyses, taking account of the latent heat exchange due to evaporation/condensation and the heat conduction in the liquid surrounding the cavity, in the same manner as Kato [7] and Plesset and Zwick [8]. We describe the outlines of these analyses in this section.

Analysis of sheet cavitation in 2-D cascade

We consider a flat plate cascade with the chordlength C, the spacing h, and the stagger angle β as shown in Fig. 1. We assume that the upstream flow has a mean velocity of U and an angle of attack α with an upstream flow rate fluctuation δN or inlet pressure fluctuation with an angular frequency of ω. We consider partial closed cavities on the suction sides of the blades with cavity length l which also fluctuates with ω. The flow disturbance due to the cavities and blades is expressed by source distributions q representing the cavities, bound vortex distributions γ_1 and γ_2 representing the blades, and trailing vortex distributions γ_t representing the wake. These singularities are distributed along the blades and their extensions downstream, assuming both steady and unsteady flow disturbances are small. Then, the complex conjugate velocity w can be written as follows.

$$w(z,t) = u - iv$$
$$= Ue^{-i\alpha} + \delta N e^{i\beta} + \frac{1}{2\pi}\left[\int_0^l (q + i\gamma_1) f(z,\xi) d\xi \right. \tag{1}$$
$$\left. + i\int_l^C \gamma_2 f(z,\xi) d\xi + i\int_C^\infty \gamma_t f(z,\xi) d\xi \right]$$
$$f(z,\xi) = \frac{\pi}{h} e^{-i(\pi/2-\beta)} \cdot \cot\left[\frac{\pi}{h}(z-\xi) e^{-i(\pi/2-\beta)}\right] + \frac{\pi}{h} e^{i\beta}$$

We introduce the following coordinates s_1 and s_2 along the cavity and the blade to take account the fluctuating cavity length.

$$\xi = l s_1 \quad (for\ 0 < \xi < l, 0 < s_1 < 1)$$
$$\xi = (C-l)s_2 + (2l - C) \quad (for\ l < \xi < C, 1 < s_2 < 2) \tag{2}$$

We define the all strength of singularities in these coordinates and divide them into steady and unsteady components as follows.

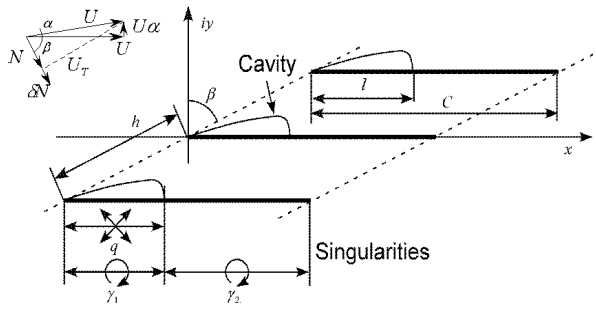

Fig.1 Model of flat plate cascade

$$
\begin{aligned}
&q(s_1,t)=q_s(s_1)+\tilde{q}(s_1)\exp j\omega t\\
&\gamma_1(s_1,t)=\gamma_{1s}(s_1)+\tilde{\gamma}_1(s_1)\exp j\omega t\\
&\gamma_2\ (s_2,t)=\gamma_{2s}(s_2)+\tilde{\gamma}_2(s_2)\exp j\omega t\\
&\gamma_t(\xi,t)=\tilde{\gamma}_t(\xi)\exp j\omega\\
&l(t)=l_s+\tilde{l}\ \exp j\omega t
\end{aligned}
\tag{3}
$$

where the imaginary unit in time j has been introduced in Eq.(3). We should note that $i{\cdot}i=j{\cdot}j=-1$ but $i{\cdot}j\neq-1$.

After substituting Eqs. (2) and (3) into Eq. (1), we divide the velocity into uniform steady velocity $Ue^{-i\alpha}$, steady disturbance (u_s, v_s) and unsteady velocity disturbance ($\tilde{u}$, $\tilde{v}$) as follows.

$$u=U+u_s+\tilde{u}e^{j\omega t},\quad v=U\alpha+v_s+\tilde{v}e^{j\omega t} \tag{4}$$

where we have assumed α<<1. We further assume that $|\tilde{u}|$, $|\tilde{v}|$ <<$|u_s|$, $|v_s|$<<U. Linearizations are made throughout the present study based on these assumptions.

The flow unknowns in Eq.(3) can be determined by the following boundary and complementary conditions, those are applied on the blade surfaces and their extensions, assuming the sufficiently thin cavity. Because the boundary and the complementary conditions for the steady components are the same as in the literature [9], we herein concentrate mainly on the unsteady components.

Boundary condition on cavity surface

We assume that the pressure on the cavity surface is equal to the vapor pressure. Under the presence of the thermodynamic effect of cavitation, the vapor pressure is locally different due to the temperature depression around the cavity surface. Applying the Clapeyron-Clausius equation to the relationship between the vapor pressure and the temperature on the cavity surface at ξ along the blade from the leading edge, we obtain,

$$\tilde{P}_V(\xi)=\frac{L}{T_\infty}\rho_V\tilde{\theta}_c(\xi)$$

where $\tilde{P}_V(\xi)$ and $\tilde{\theta}_c(\xi)$ respectively denote the amplitudes of unsteady vapor pressure and temperature on the cavity surface, and L, ρ_V and T_∞ are the latent heat of evaporation, the density of vapor phase and the temperature at the upstream infinity. Substituting the above equation into the linearized momentum equation on the cavity surface, we obtain;

$$j\omega\frac{\tilde{u}_c'(\xi)}{U}+\frac{\partial}{\partial\xi}\left(\frac{\tilde{u}_c'(\xi)}{U}\right)=-\left(\frac{\rho_V}{\rho_L}\right)\frac{L}{U^2}\left(\frac{\tilde{\theta}_c(\xi)}{T_\infty}\right) \tag{5}$$

By using $\tilde{u}_c'(\xi)$, the boundary condition on the cavity surface in the coordinate fixed to the fluctuating cavity can be expressed as follows.

$$\tilde{u}(ls_1+0i)=\tilde{u}_c(s_1)=\tilde{u}_c'(l_ss_1)+s_1\frac{du_{cs}}{ds_1}\frac{\tilde{l}}{l_s} \tag{6}$$

where $u_{cs}(s_1)$ denotes the steady component of the velocity on the cavity surface and $\tilde{u}_c(s_1)$ denotes the amplitude of the unsteady velocity on the cavity surface defined in the coordinate fixed to the fluctuating cavity.

Boundary condition on wetted surface

We employ the following flow tangency condition on the wetted blade surfaces.

$$
\begin{aligned}
&\tilde{v}(ls_1+0i)=0\\
&\tilde{v}\left[(C-l)s_2+2(l-C)\pm0i\right]=0
\end{aligned}
\tag{7}
$$

Kutta's condition

We assume that the pressure difference across the blade vanishes at the trailing edge. This condition can be obtained by applying the linearized momentum equation on both surfaces of the blades and expressed as follows.

$$\frac{d}{dt}\left[\int_0^1\gamma_1(s_1,t)lds_1+\int_1^2\gamma_2(s_2,t)(C-l)ds_2\right]+U\cdot\gamma_2(2,t)=0$$

This equation is equivalent to the Kelvin's circulation conservation law and determines the strength of free vortex $\gamma_2(2,\ t)$ shed on the main flow U from the trailing edge in accordance with the change in the blade circulation. Assuming that the trailing free vortices are transported by the main flow U, we obtain the following free vortex distribution.

$$\tilde{\gamma}_t=\tilde{\gamma}_2(2)\exp\left[-j\omega(\xi-C)/U\right] \tag{8}$$

Cavity closure condition

We employ the closed cavity model for its simplicity. The cavity thickness $\eta(s_1,\ t)$ should be determined to satisfy the following kinematic boundary condition on the cavity surface.

$$\frac{\partial\eta}{\partial t}+\frac{1}{l}\left(U-s_1\frac{dl}{dt}\right)\frac{\partial\eta}{\partial s_1}=v(ls_1+0i)=q(s_1,t)$$

After dividing this equation into the steady and unsteady parts we linearize and integrate them. Then, we can obtain the steady and unsteady components of cavity thickness. The unsteady cavity thickness $\tilde{\eta}(s_1)$ is expressed as follows.

$$
\begin{aligned}
\tilde{\eta}(s_1)=&\frac{l_s}{U}\int_0^{s_1}\tilde{q}(s_1')e^{-j\omega l_s(s_1-s_1')/U}ds_1'\\
&+\frac{\tilde{l}}{U}\int_0^{s_1}(1+j\omega l_ss_1'U)q_s(s_1')e^{-j\omega l_s(s_1-s_1')/U}ds_1'
\end{aligned}
$$

Imposing the condition of zero cavity thickness at the trailing edge of cavity, we obtain the following cavity closure condition.

$$\tilde{\eta}(1)=0 \tag{9}$$

Inlet pressure condition

This condition can be derived by integrating the linearized momentum equation in x-direction from far upstream (x=-∞) to the leading edge of the cavity (x=0). For the unsteady components, we obtain following equations.

$$-j\omega\int_{-\infty}^0x\frac{\partial\tilde{u}}{\partial x}dx+U\tilde{u}_c'(0)=\frac{\tilde{p}_0}{\rho} \tag{10}$$

where

$$\tilde{p}_0=\tilde{p}_{-\infty}+j\rho\omega\lim_{x\to-\infty}x\tilde{u}$$

corresponds to the pressure fluctuation at the cascade inlet.

Heat exchange between cavity and surrounding liquid

We assume that the flow inside the cavity is uniform in the y-direction with the velocity on the cavity surface. Considering the continuity relation in the small control volume inside the cavity as shown in Fig. 2, we can relate the local evaporation velocity V with the source distribution q as follows.

$$V = -\left[\frac{\partial \eta}{\partial t} + \frac{1}{l}\left(U - s_1 \frac{dl}{dt}\right)\frac{\partial \eta_0}{\partial s_1}\right] = -q(s_1, t)$$

Then, the unsteady heat flux $\tilde{q}_T(s_1)$ across the cavity surface, defined in the coordinate fixed to the cavity, can be related with the unsteady source distribution $\tilde{q}(s_1)$ as follows.

$$\tilde{q}_T(s_1) = \rho_V L \tilde{V} = -\rho_V L \tilde{q}(s_1)$$

where L denotes the latent heat of evaporation.

Due to the heat flux across the cavity surface, there appears a temperature distribution around the cavity. We assume that the heat conduction in the main flow direction (x) is negligibly small and treat here only that in the normal direction (y) of the cavity surface. The temperature increase (decrease) ΔT due to the formation of thin cavity should satisfy the following linearized energy equation for inviscid flow.

$$\frac{\partial \Delta T}{\partial t} + U\frac{\partial \Delta T}{\partial x} = \varepsilon a \frac{\partial^2 \Delta T}{\partial y^2}$$

where a denotes a thermal diffusivity. Kato's turbulent diffusivity factor ε [7] has been employed to take account of the enhancement of thermal diffusion due to the turbulent flow around the cavity.

We divide the temperature increase ΔT into steady and unsteady components. Solving analytically the above energy equation under the boundary condition of ΔT=0 at the leading edge of the cavity, we obtain the amplitude of unsteady temperature increase $\tilde{\theta}(x, y)$ as follows.

$$\tilde{\theta}(x,y) = \frac{y}{2\sqrt{\pi \kappa_p}} \int_0^x \tilde{\theta}_c(\xi) e^{-j\frac{\omega}{U}(x-\xi)} \frac{\exp\left(-\frac{y^2}{4K_p(x-\xi)}\right)}{(x-\xi)^{3/2}} d\xi$$

where $\tilde{\theta}_c(\xi)$ denotes the amplitude of the unsteady temperature on the cavity surface. K_p is defined here as $K_p = \varepsilon a/U$. Then, the temperature gradient normal to the cavity surface is derived as

$$\lim_{y\to 0} \frac{d\tilde{\theta}(x,y)}{dy} = -\frac{1}{\sqrt{\pi K_P}} \int_0^x \left[\frac{d\tilde{\theta}_c(\xi)}{d\xi} + j\frac{\omega}{U}\tilde{\theta}_c(\xi)\right] \frac{e^{-j\frac{\omega}{U}(x-\xi)}}{(x-\xi)^{1/2}} d\xi$$

By using Fourier's theorem, $q_T = -\varepsilon\lambda(\partial T/\partial y)|_{y=0}$, we obtain the following equation.

$$\int_0^x \left[\frac{d\tilde{\theta}_c(\xi)}{d\xi} + j\frac{\omega}{U}\tilde{\theta}_c(\xi)\right] \frac{e^{-j\frac{\omega}{U}(x-\xi)}}{T_\infty (x-\xi)^{-1/2}} d\xi = -\frac{L}{c_{pl}T_\infty}\left(\frac{\rho_V}{\rho_L}\right)\sqrt{\frac{\pi}{K_P}}\left[\frac{\tilde{q}}{U} - \frac{s_1}{U}\frac{dq_s}{ds_1}\frac{\tilde{l}}{l_s}\right] \tag{11}$$

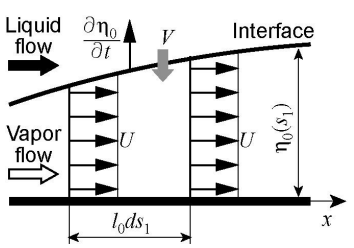

Fig.2 Control volume for continuity equation

Cavitation compliance and mass flow gain factor

The unknown quantities in this problem are the steady and unsteady components of $q(s_1,t)$, $\gamma_1(s_1,t)$, $\gamma_2(s_1,t)$, $\gamma_t(\xi,t)$, $l(t)$, $u_c(s_1,t)$ and $\Delta T(\xi,t)$. Descretizations of singularities distributed along the blades and cavities are made in the same manner as in the previous report [5], where nodes are distributed more densely near the leading and trailing edges of the blades and cavities. The control points, where boundary conditions are applied, are placed at the midpoints between each node.

The analytical method to obtain the steady components is the same as that described in the previous report [9], and it has been found that the results are expressed by using $\sigma/2\alpha$, where σ is a cavitation number defined as $\sigma = 2[P_\infty - P_v(T_\infty)]/\rho_L U^2$.

The unsteady components are determined from the boundary and complementary conditions Eqs. (5)-(11). After the descritiztations, we obtain a set of linear equations for the unsteady components as follows.

$$\begin{aligned} &[A_u(l_s,\omega)]\tilde{Q} = B_u(\tilde{p}_0, \tilde{N}) \\ &\tilde{Q} = \{\tilde{q}, \cdots, \tilde{\gamma}_1, \cdots, \tilde{\gamma}_2, \cdots, \tilde{\gamma}_t, \alpha\tilde{l}, \tilde{u}_c, \cdots, \tilde{\theta}_c, \cdots\}^T \end{aligned} \tag{12}$$

By solving this equation, we can obtain the response of the flow field against the inlet pressure fluctuation $\tilde{p}_0$ or the flow rate fluctuation $\tilde{N}$. Once the flow field is determined, the cavity volume fluctuation can be calculated by the following equation, which is derived by integrating the cavity thickness along the blade.

$$\begin{aligned} \tilde{V}_c &= \frac{l_s^2}{U}\int_0^1 \int_0^{s_1} \tilde{q}(s_1') e^{-j\omega l_s (s_1 - s_1')/U} ds_1' ds_1 \\ &+ \frac{\tilde{l}}{l_s}\frac{l_s^2}{U}\int_0^1 \int_0^{s_1} (1 + j\omega j_s/U) q(s_1') e^{-j\omega l_s (s_1 - s_1')/U} ds_1' ds_1 \\ &- \frac{\tilde{l}}{l_s}\frac{l_s^2}{U}\int_0^1 s_1 q(s_1) ds_1 \end{aligned}$$

Then, the cavitation compliance K and the mass flow gain factor M can be calculated by the following equations.

$$\begin{aligned} K &= -\frac{\partial V_c/h^2}{\partial \sigma} = -\frac{(\tilde{V}_c/h^2)_{\tilde{N}=0}}{2\tilde{p}_0/\rho U^2} \\ M &= -\frac{\partial V_c/h^2}{\partial N/U} = -\frac{(\tilde{V}_c/h^2)_{\tilde{p}_0=0}}{\tilde{N}/U} \end{aligned} \tag{13}$$

We can find from Eqs. (5) and (11) that the thermodynamic effect of cavitation can be represented by the following thermodynamic parameter Σ^*.

$$\Sigma^* = \frac{L^2}{c_{pl}T_\infty}\left(\frac{\rho_V}{\rho_L}\right)^2 \sqrt{\frac{C}{aU^3}} \tag{14}$$

The parameter Σ^* is identical to that proposed by Brennen [10], who derived it by considering the thermodynamics of the traveling vapor bubble along the suction side of the blade. This fact implies that the parameter Σ^* is a primary thermodynamic parameter also for the film-like cavitation developed on the suction side of the blade. And also, because the unknowns representing the steady flow, including the cavity length l_s, have been found to functions of $\sigma/2\alpha$ and Σ^* [9], we can conclude from Eqs. (12) and (13) that the unsteady cavitating flow field as well as the cavitation characteristics K and M are the functions of $\sigma/2\alpha$ and Σ^*.

Analysis of tip leakage vortex cavitation

We construct a simple analytical model considering the thermodynamic effect of tip leakage vortex cavitation using a slender body approximation. The base model has been developed by Watanabe et al. [11] and Higashi et al. [12] by coupling two-dimensional vortex method in cross flow plane with a two-dimensional version of Rayleigh Plesset equation for a cylindrical vapor bubble without the thermodynamic effect. We implemented the thermodynamic effect into the bubble radius equation of the base model by taking account of the latent heat of evaporation and the heat diffusion in the liquid phase around the cavity. Details in the analysis are given in this subsection.

Slender body approximation

The tip leakage vortex cavitation occurs in the low pressure region in the core of the tip leakage vortex formed by rolling up of the shear layer between the leakage flow and the main flow. The tip leakage vortex forms as a sort of longitudinal vortex, and the slender body approximation has been found to be useful for the analysis of the tip leakage vortex (Rains [13], Chen et al. [14]) and cavitation in it (Higashi et al. [12].) We also herein use the slender body approximation, assuming that the flow variations in the main flow direction are sufficiently small compared to those in the cross flow plane.

Figure 3 illustrates the conceptual figure of the slender body approximation. Cross flow planes A, B, C and D at different chordwise locations are shown as examples. The cross flow planes A and D respectively include the leading and trailing edges of the blade. The blade has a clearance against one of the end walls. Main flow comes with the velocity of U and the attack angle of α. A tip leakage vortex initiates near the leading edge of the suction side of the blade and develops along the chordwise direction as shown in this figure. We assume that every fluid particle in the cross flow plane moves through the blade with the velocity U of the main flow. Hence the distance between the cross planes to be analyzed is $\Delta S=U\cdot\Delta t$ where Δt is a time increment. Then the steady three-dimensional flow is converted to the unsteady two-dimensional cross flow as shown in Fig. 4.

Cross flow analysis using 2-D vortex method

We employ a two dimensional vortex method for the unsteady cross flow analysis. The model is shown in Fig. 5. We express the tip leakage flow by the source term $q_J(t)=2\cdot U_J(t)$

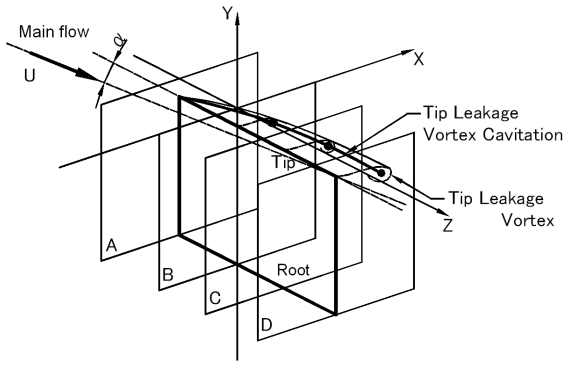

Fig. 3 Concept of slender body approximation

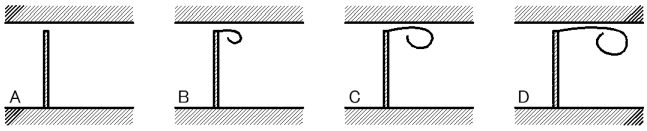

Fig. 4 Images of tip leakage vortex in cross plane

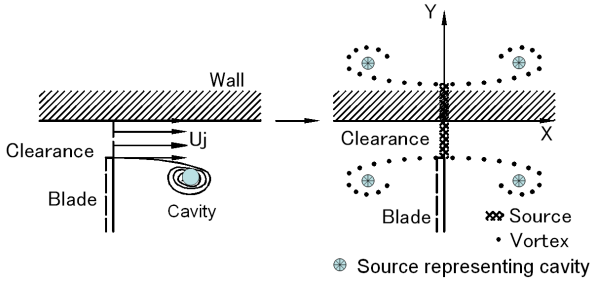

Fig. 5 Two dimensional vortex method

distributed uniformly along the tip clearance ($z=iy$, $-\tau<y<0$), where $U_J(t)$ is a leakage velocity. The discrete free vortices representing the shear layer between the main flow and the leakage flow is shed from the tip of the blade at every time step with the magnitude of $\gamma_J(t)=U_J^2\Delta t/2$. The velocity of the tip leakage flow in the cross plane is simply calculated from $U_J(t)/U=[\Delta C_p(Ut)]^{1/2}$, where $\Delta C_p(S=Ut)$ represents the coefficient of the pressure difference across the blade. Figure 6 shows the pressure coefficient distributions of the flat plate hydrofoil with the attack angle of α=4°, which is obtained by an inviscid flow analysis. Note that C_{pmin} is set to be $-\sigma$, where $\sigma=2(p_\infty-p_v)/\rho_l U^2$ (p_∞: upstream pressure, p_v: vapor pressure, ρ_L: density of liquid phase) is the cavitation number, assuming the pressure cannot be lower than the vapor pressure.

After the inception of a cavitation bubble, we have to consider another source term q_B due to the growth and shrinkage of the cavitation bubble. This term is determined by $q_B=2\pi R\cdot DR/Dt$ once the bubble radius $R(t)$ and the bubble radius velocity $DR/Dt(t)$ are determined from the bubble radius equation described later.

The boundary conditions on the rigid surfaces of the tip end and the blade walls are satisfied by introducing the mirror images of all singularities as shown in Fig. 5. However, the mirror images with respect to the blade walls are not considered downstream of the blade ($S>C$, C: chordlength). The effect of

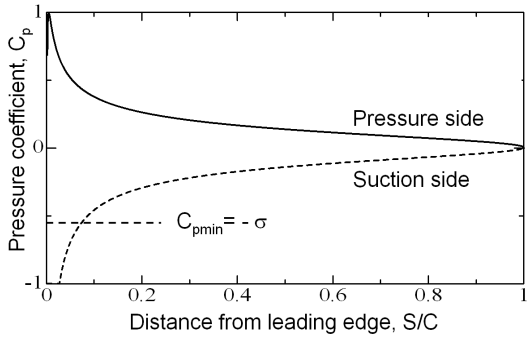

Fig. 6 Pressure distribution along flat plate blade

the end wall of blade root is ignored since the root end wall is sufficiently far from the tip leakage vortex.

Bubble radius equation

It is assumed that a single cylindrical bubble with the initial radius of R_0 starts to develop at the location of the center of the vortex core at the moment when the pressure there becomes lower than the vapor pressure. The growth of the cylindrical bubble radius R and its time derivative DR/Dt are calculated by the bubble radius equation. The cylindrical bubble radius equation, which is similar to Rayleigh Plesset equation for spherical bubble, is derived from the unsteady Bernoulli's equation. We apply the unsteady Bernoulli's equation between the bubble surface and the root of the suction surface of the blade with the assumption of the small bubble radius. By setting the pressure at the bubble surface to be a vapor pressure, we obtain the bubble radius equation in the following form.

$$\frac{d^2R^*}{dt^{*2}} = f\left(R^*, \frac{dR^*}{dt^*}, C_{ps}, \sigma, \Delta p_v^*, \cdots\right) \tag{15}$$

where * denotes the non-dimensional value using the chordlength C and main flow velocity U as the representative length and velocity, and C_{ps} denotes the pressure coefficient of the suction surface of the blade. The value ΔP_v^* denotes the non-dimensional value of the vapor pressure difference between upstream temperature and the local temperature on the bubble surface. In the case without the thermodynamic effect of cavitation, ΔP_v^* diminishes since the temperature is constant over the entire flow field, whereas, in other cases, ΔP_v^* becomes significant because the temperature around the cavity decreases due to the latent heat of evaporation, which is modeled in the following subsection.

Implementation of thermodynamic effect of cavitation

The thermodynamic effect is now considered in the same manner as proposed by Plesset and Zwick [8], who solve the heat diffusion equation around a spherical vapor bubble under the assumption of the small temperature boundary layer thickness compared with the bubble radius. We also solve the temperature diffusion equation around a cylindrical bubble and equate the heat flux on the cavity surface with the latent heat of evaporation per unit surface area and unit time. As a result, we obtain the following temperature depression term.

$$\frac{T_\infty - T_C}{\rho_v L / \rho_l c_{pl}} = \sqrt{\frac{CU}{a\varepsilon}} J \tag{16}$$

$$J = \frac{1}{\sqrt{\pi}} \int_0^t \frac{R(x)\dfrac{DR}{Dt}(x)}{\left[\int_x^t R(y)^2 dy\right]^{1/2}} dx \tag{17}$$

where T_C, ρ_v, L, c_{pl} and a denote the temperature on the cavity surface, the density of the vapor phase, the latent heat of evaporation, the liquid heat capacity and the thermal diffusivity respectively. The turbulent diffusion factor ε has been again introduced. Assuming the thermodynamically equilibrium state, we employ Clapeyron-Clausius equation to relate the temperature depression with the vapor pressure change.

$$\Delta p_v^* = \frac{p_v(T_\infty) - p_v(T_C)}{\rho_l U^2/2} = \frac{dp_v/dT}{\rho_l U^2/2}(T_\infty - T_C) = \Sigma^* \sqrt{\frac{1}{\varepsilon}} J \tag{18}$$

The parameter Σ^* in this equation is completely the same as that defined by Eq.(14), which is derived for sheet cavitation of the hydrofoil. This fact implies that the parameter Σ^* is a primary thermodynamic parameter for not only the sheet cavitation but also the tip leakage vortex cavitation.

RESULTS AND DISCUSSIONS

Sheet cavitation of 2-D cascade

In the analysis of sheet cavitation, geometrical parameters of cascade are set as the solidity of C/h=2.0, the stagger of β=75.0° as a model for inducers. The angle of attack α=5.0° is used when needed. Since it has been found that the thermodynamic parameter Σ^* roughly takes the values among 0-1000 [5], we set Σ^*=0 (no thermodynamic effect), 20, 40 and 100. The turbulent diffusion factor ε is unknown but set to be 4000, which is the identical value used in the previous study [5].

We have confirmed that the results for Σ^*=0 agrees with those obtained by Otsuka et al. [4], who calculated the cavitation compliance and the mass flow gain factor without considering the thermodynamic effect.

Quasi-steady cavitation characteristics

Figure 7 shows the steady cavity length l_s/h plotted against $\sigma/2\alpha$. Figure 8 shows the quasi-steady values of the cavitation compliance K and the mass flow gain factor M plotted against (a) $\sigma/2\alpha$ and (b) the steady cavity length l_s/h. We can find from Fig. 7 that, as Σ^* increases, namely the thermodynamic effects becomes significant, the cavity becomes shorter for the same value of $\sigma/2\alpha$. Especially, in the case with Σ^*=100, we have the short sheet cavity with l_s/h <1.0 even at $\sigma/2\alpha$ =0. At the same time, we can find from Fig. 8(a) that the quasi-steady values of K and M take smaller values as Σ^* increases. However, looking at Fig. 8 (b), we can find that, for the shorter cavity with l_s/h <1.0, the quasi steady values of both K and M do not significantly change with the increase of Σ^*. This means that, for the shorter cavity, the quasi steady values of both K and M depend only on the cavity length, and the thermodynamic effect affects those values only through the cavity length. On the other hand, if the cavity becomes longer, whose cavity length is larger than the blade spacing h, l_s/h >1.0, the quasi-steady

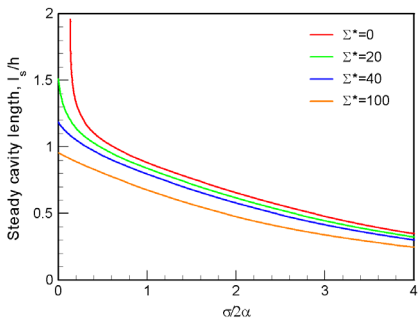

Fig. 7 Steady cavity length vs. $\sigma/2\alpha$

values of K and M become smaller as Σ^* increases. This trend seems to be more significant in the mass flow fain factor M than in the cavitation compliance K. This fact might imply that the onset region of cavitation instabilities becomes smaller with the thermodynamic effect of cavitation, considering that the cause of the cavitation instabilities could be explained by the positive mass flow gain factor, M>0 [1].

Figure 9 shows the steady cavity shapes with Σ*=0 and 100 for various steady cavity lengths of (a) l_s/h =0.6, (b) 1.0 and (c) 1.4. We can find that, due to the thermodynamic effect of cavitation, the cavity becomes thicker near the leading edge and thinner near the trailing edge in all cases. Thinner is the cavity near the trailing edge, the interaction between the flow around the cavity trailing edge and that around the leading edge of the adjacent blade is considered to become weaker, which seems to explain the previous result that the thermodynamic effect is significant in K and M for longer cavity with l_s/h >1.0.

Unsteady cavitation characteristics

Figure 10 shows example results of unsteady values of cavitation compliance and mass flow gain factor for (a) l_s/h =0.2, (b) 0.6 and (c) 1.0. In these figures, the complex values of K and M normalized by their quasi-steady values are plotted in the complex plane. When the imaginary part of K (or M) takes the negative value, the response of the cavity volume delays against the imposed inlet pressure (or flow rate) fluctuation. The value $k=\omega h/U$ in the figures denotes the normalized frequency. Generally, the phase delay of the cavity response against the imposed fluctuation becomes larger as the normalized frequency k is increased, except for some peculiar cases.

At first, for shorter cavity, whose cavity length is sufficiently smaller than the blade spacing h, the thermodynamic effect hardly affects the cavitation compliance K and the mass flow gain factor M as shown in Fig. 10 (a). Next, when the cavity becomes longer and the cavity length approaches to the 60% of the blade spacing, the thermodynamic effect begins to affect the cavitation compliance K as shown in Fig. 10 (b). When the trailing edge of the cavity approaches the inlet throat of the blade passage, the thermodynamic effect significantly affects both K and M as shown in Fig. 10 (c), Looking more carefully at Fig. 10 (c), we can find that only K takes the positive imaginary part for lower normalized frequency k. This means that there is a phase advance in the cavity volume response against the inlet pressure fluctuation.

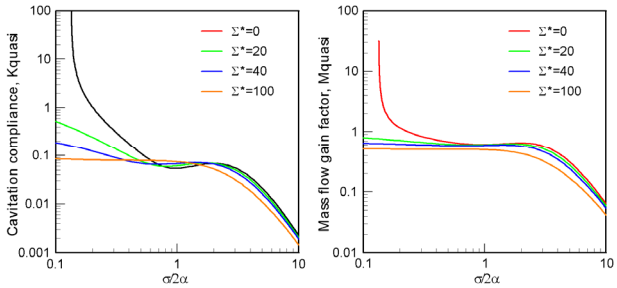

(a) (K, M) vs. $\sigma/2\alpha$

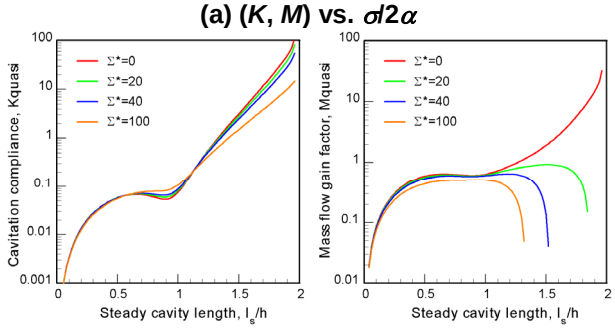

(b) (K, M) vs. steady cavity length

Fig. 8 Quasi-steady cavitation compliance and mass flow gain factor

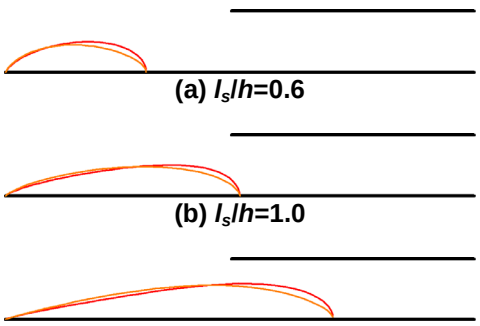

(a) l_s/h=0.6

(b) l_s/h=1.0

(c) l_s/h=1.4

Fig. 9 Steady cavity shapes for various cavity lengths (red: Σ*=0.0, orange: Σ*=100.0)

From Fig. 10 (c), we can find that this phase advance becomes smaller as Σ^* increases.

By the way, it is well known from [1] that the positive value of M enhances the occurrence of the cavitation instabilities, while the positive value of K suppresses it. Let us consider the one-dimensional oscillation mode in a duct like the cavitation surge mode. The pressure fluctuation in the duct flow takes the phase delay of about 90 degrees against the flow rate fluctuation. Then, the positive imaginary parts of K and M respectively work as the positive mass flow gain factor and the negative cavitation compliance. Looking again at Fig. 10 (c), the positive imaginary part in K can be seen with small normalized frequencies, which could equivalently increase the mass flow gain factor and enhance the occurrence of the cavitation surge. As Σ^* increases, the imaginary part of K decreases and becomes negative in the case with Σ^*=100, indicating that the equivalent mass flow gain factor decreases with the increase of Σ^*. This again might imply that the onset

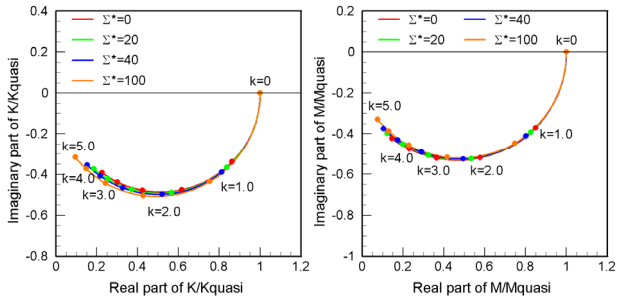

(a) l_s/h=0.2

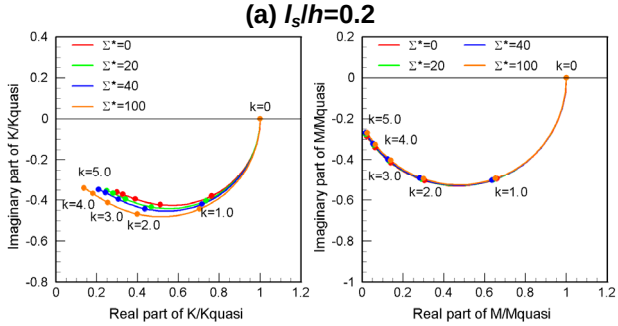

(b) l_s/h=0.6

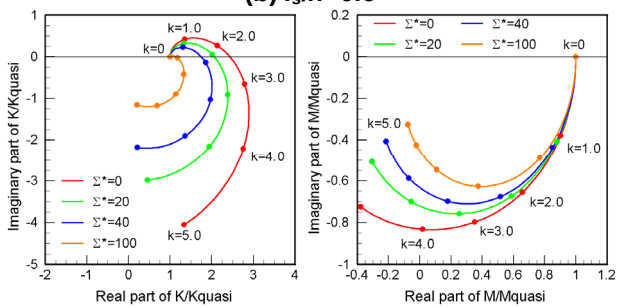

(c) l_s/h=1.0

Fig. 10 Unsteady cavitation compliance and mass flow gain factor

region of cavitation instabilities becomes smaller with the thermodynamic effect of cavitation.

Tip leakage vortex cavitation

We apply our method to the tip leakage vortex cavitation of an isolated flat plate hydrofoil, whose chordlength of C=90 mm, the span length of B=67 mm and the tip clearance of τ=3 mm. We set the main flow with the velocity of U=10 m/s and the attack angle of α=4.0, 5.0 and 6.0°, and the various values of the cavitation number σ. On the thermodynamic parameter Σ^*, we set Σ^*=0 (no thermodynamic effect), 10 and 100. The turbulent diffusion factor ε is set to be 1000 through the present calculations.

The time increment and the initial bubble radius are set to be Δt=0.001C/U and R_0=0.00001C. We have confirmed that the present analysis well simulate the cavity shape of the tip leakage vortex cavitation in the case without the thermodynamic effect of cavitation [6]. The validations with thermo-sensible fluids are necessary but have not yet been done since there is no available data. Then, in the present study, we discuss only the qualitative aspect of the thermodynamic effect on the tip leakage vortex cavitation.

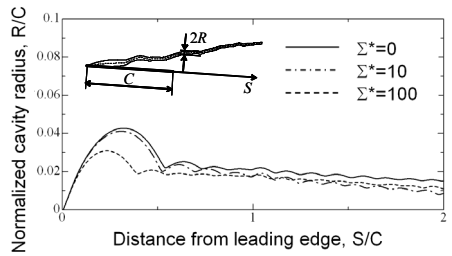

(a) Cavity radius

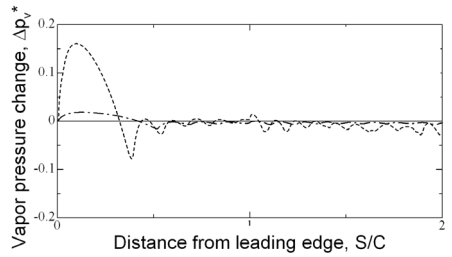

(b) Vapor pressure change

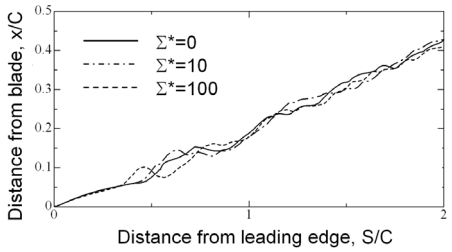

(c) x-location of center of cavity

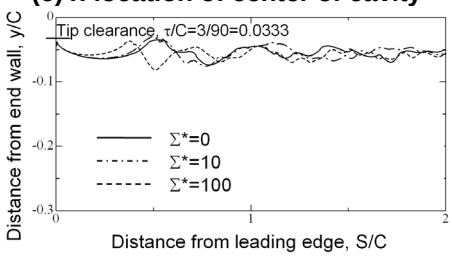

(d) y-location of cavity

Fig. 11 Cavity radius, vapor pressure change and trajectory of the cavity center with thermodynamic effect (σ=1.0, α=4.0°)

Thermodynamic effect of tip leakage vortex cavitation

Firstly, we would like to show the example results of the tip leakage vortex cavitation with the thermodynamic effect of cavitation. The cavitation number and the angle of attack are σ=1.0 and α=4.0°. Figure 11 shows (a) the cross-sectional cavity radius distribution R/C and (b) the vapor pressure depression Δp_v^* along the vortex axis. We can find that the cavity rapidly develops just after its inception and takes the maximum radius at around S/C=0.25-0.3. Then the cavity starts to collapse rapidly whereas, after the first collapse, the change of the cavity radius becomes gradual. Focusing on the effect of the thermodynamic parameter Σ^*, we can see that the maximum radius of the cavity becomes significantly smaller as the thermodynamic parameter Σ^* is increased, which is due to the

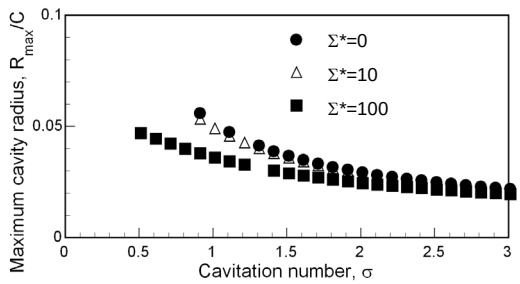

(a) Maximum cavity radius

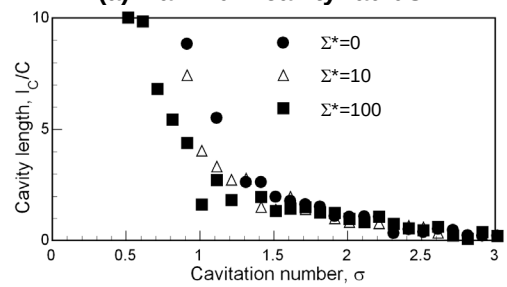

(b) Cavity length

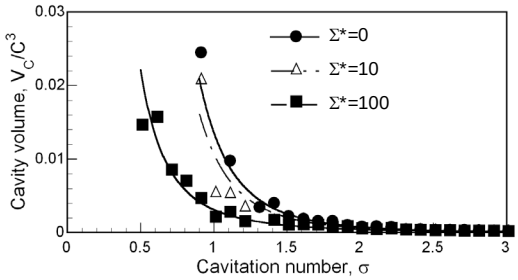

(c) Cavity volume

Fig. 12 Thermodynamic effect on the geometries of tip vortex cavity (α=5.0°)

temperature, i.e., the vapor pressure depression as shown in Fig. 11 (b). The thermodynamic effect is more remarkable there, because we have a large latent heat of evaporation due to the rapid growth of the cavity. On the other hand, after the first collapse, the cavity radius dose not change very much for the different values of Σ^*, and the vapor pressure depression is small in this region.

The trajectory of the cavity is plotted in Figs. 11 (c) and (d), and we can find that the trajectory is not significantly affected by the thermodynamic effect of cavitation.

Next, Fig. 12 summarizes the shape of the tip leakage vortex cavity by showing the maximum cavity radius R_{max}/C, the cavity length l/C and the cavity volume V_c/C^3 plotted against the cavitation number. The angle of attack is α=5.0°. The maximum cavity radius means the maximum radius of the cross-section of the cavity along the vortex axis. The cavity length is measured as the distance between the locations of the inception and the final collapse of the cavity. The cavity volume is calculated by integrating the cavity cross sectional area πR^2 from the leading edge to the trailing edge of the cavity. We can see in Fig. 12 (a) that the maximum radius increases with the decrease of the cavitation number for all values of Σ^*. As the thermodynamic parameter Σ^* increases, the maximum cavity radius decreases especially for smaller cavitation number,

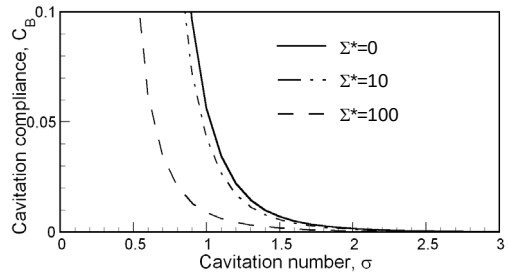

(a) Cavitation compliance

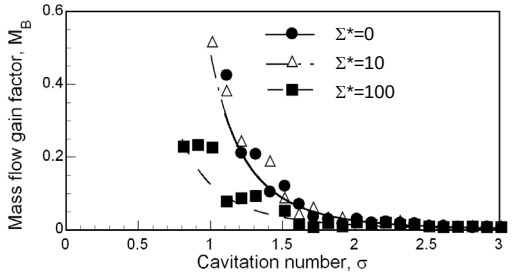

(b) Mass flow gain factor

Fig. 13 Quasi-steady cavitation compliance and mass flow gain factor of tip leakage vortex cavity (α=5.0°)

which is because of the thermodynamic effect of cavitation. For larger cavitation number, the thermodynamic effect is very small and seems to be negligible, which is probably because the cavity is small. Looking at the cavity length in Fig. 12 (b), although the plots are scattered for smaller cavitation number, we can find that the cavity becomes shorter as the thermodynamic parameter Σ^* increases in the smaller cavitation number range. For larger cavitation number, the cavity length does not change very much with the increase of Σ^*, meaning again that the thermodynamic effect seems to be negligible. The cavity volume shown in Fig. 12 (c) has the same tendency as those in the maximum cavity radius and the cavity length.

Cavitation compliance and mass flow gain factor

Here, we define the cavitation compliance C_B and the mass flow gain factor M_B of the tip leakage vortex cavitation as follows.

$$C_B = -\frac{\partial V_C / C^3}{\partial \sigma}, \; M_B = \frac{\partial V_C / C^3}{\partial \alpha} \tag{19}$$

Figure 13 shows the quasi-steady cavitation compliance C_B and the quasi-steady mass flow gain factor M_B for various cavitation numbers with the attack angle of α=5.0°. In the present study, C_B is calculated by differentiating the fitting curve of the cavity volume shown in Fig. 12 (c). M_B is obtained by calculating the finite deference of the cavity volume between the results of α=4.0° and 6.0° with the constant cavitation number. We can see that both C_B and M_B increase with the decrease of the cavitation number for all values of Σ^*. It is a little hard to see because of the scattered symbols, but by comparing the results between Σ^*=0 and 100, we can find that the thermodynamic effect reduces both C_B and M_B. This is simply because the cavity volume decreases with the thermodynamic effect of cavitation as shown in Fig. 12 (c).

CONCLUSIONS

In the present study, the cavitation characteristics, the cavitation compliance K (or C_B) and the mass flow gain factor M (or M_B), are estimated for the partial cavitation in a 2-D flat plate cascade and the tip leakage vortex cavitation of an isolated flat plate hydrofoil by simple analyses based on the potential flow theory considering the thermodynamic effect of cavitation. Main results are summarized as follows.

(a) It is shown that the thermodynamic effect can be included in the analysis only thorough one thermodynamic parameter Σ^* for both the sheet cavitation and the tip leakage vortex cavitation. The cavitation compliance and mass flow gain factor are functions of $\sigma/2\alpha$ (or the steady cavity length l_s/h) and Σ^*.

(b) The quasi-steady values of K and M of sheet cavitation are drastically decreased when the cavity length exceeds approximately the blade spacing. This is seen more significantly in M.

(c) The unsteady values of K and M are also drastically changed when the cavity length exceeds approximately the blade spacing. Especially, the phase advance in K observed with longer cavity and smaller imposed frequency decreases with the increase of Σ^*.

(d) From both the quasi-steady and unsteady values of K and M, it is expected that the thermodynamic effect of cavitation suppresses the occurrence of cavitation instabilities, considering the fact that their onset conditions are explained by $M>0$.

(e) The cavitation compliance C_B and the mass flow gain factor M_B of the tip leakage vortex cavitation are calculated quasi-statically from the steady cavity volume. Both of them are decreased by the thermodynamic effect of cavitation.

This study is partly supported by the Grant-in-Aid for Scientific Research for the Ministry of Education, Science, Sports and Culture.

REFERENCES

[1] Tsujimoto, Y., Kamijo, K. and Brennen, C.E., 2001, “Unified Treatment of Flow Instabilities of Turbomachines,” *AIAA J. Propulsion and Power*, 17, No.3, 636-643

[2] Brennen, C. E., 1978, “Bubbly Flow Model for the Dynamic Characteristic of Cavitating Pumps,” Journal of Fluid Mechanics, Vol. 89, pp.223-240.

[3] Nishiyama, H. and Nishiyama. T., 1980, “Dynamic Transfer Characteristics of Partially Cavitated Hydrofoil Cascade,” Proc. IAHR Symposium, Tokyo, pp.234-254.

[4] Otsuka, S., Tsujimoto, Y., Kamijo, K and Furuya, O., 1996, “Frequency Dependence of Mass Flow Gain Factor and Cavitation Compliance of Cavitating Inducer,” ASME J. Fluids Eng., Vol.118, pp. 400-408.

[5] Watanabe, S., Hidaka, T., Horiguchi, H., Furukawa, A. and Tsujimoto, Y., 2007, “Analysis of Thermodynamic Effects on Cavitation Instabilities,” ASME J. Fluids Eng., Vol. 129, pp. 1123-1130.

[6] Watanabe, S., Ikeda, A., Furukawa, A. and Nishii, K., 2008, “An Analysis of Thermodynamic Effect of Tip Leakage Vortex Cavitation,” Proc. of WIMRC Cavitation Forum 2008,

[7] Kato, H., 1984, “Thermodynamic Effect on Incipient and Development of Sheet Cavitation,” *ASME* FED-Vol.16, 127-136.

[8] Plesset, M. S. and Zwick S. A., 1954, "The Growth of Vapor Bubbles in Superheated Liquids," J. Appl. Phys., Vol. 25, pp. 493-500.

[9] Watanabe, S., Hidaka, T., Horiguchi, H., Furukawa, A. and Tsujimoto, Y., 2007, “Steady Analysis of the Thermodynamic Effects of Partial Cavitation Using the Singularity Method,” ASME J. Fluids Eng., Vol. 129, pp. 121-127.

[10] Brennen, C. E., 1994, *Hydrodynamics of Pumps*, Concepts ETI, Inc and Oxford University Press.

[11] Watanabe, S., Seki, H., Higashi, S., Yokota, K. and Tsujimoto, Y., 2001, "Modeling of 2-D Leakage Jet Cavitation as a Basic Study of Tip Leakage Vortex Cavitation," ASME J. Fluids Eng., Vol. 123, pp. 50-56.

[12] Higashi, S., Yoshida, Y. and Tsujimoto, Y., 2002, "Tip Leakage Vortex Cavitation from the Tip Clearance of a Single Hydrofoil," *JSME Int. J., Ser. B*, Vol. 45, 662-671.

[13] Rains, D. A., 1954, "Tip Clearance Flows in Axial Compressors and Pumps," California Institute of Technology, Hydrodynamics and Mechanical Engineering Laboratories Report No. 5.

[14] Chen, G. T., Greitzer, E. M., Tan, C. S. and Marble, F. E., 1991, “Similarity Analysis of Compressor Tip Clearance Flow Structure,” ASME Journal of Turbomachinery, Vol. 113, pp. 260-271.